Math 673

Multigrid Methods: A Mostly Matrix-Based Approach

Chapter 03: Fourier Analysis of the Two-Grid Algorithm

Abner J. Salgado and Steven M. Wise

asalgad1@utk.edu — swise1@.utk.edu
University of Tennessee

Fall 2024

Chapter 03, Part 3 of 3

Fourier Analysis of the Two-Grid Algorithm

Other Restriction Matrices

Other Restriction Matrices

The prolongation matrix makes good geometric sense. If $\boldsymbol{u}_0 \in \mathbb{R}^{n_0}$ is the unique coordinate vector of the function $u_0 \in V_0$ with respect to the basis B_0, then $\mathrm{P}_0\boldsymbol{u}_0$ is its unique coordinate vector in the basis B_1. But what is the interpretation of the restriction matrix?

Consider the fine grid function, $u_1 \in V_1$, pictured in Figure 1, where $n_1 = 7$. Suppose its coordinate vector in the basis B_1 is represented as $\boldsymbol{u}_1 \in \mathbb{R}^7$. Let $R_0 u_1 \in V_0$ ($\frac{1}{2} R_0 u_1 \in V_0$) be the function whose coordinate representation in the basis B_0 is $\mathrm{R}_0\boldsymbol{u}_1$ ($\frac{1}{2}\mathrm{R}_0\boldsymbol{u}_1$). See the figure on the next slide.

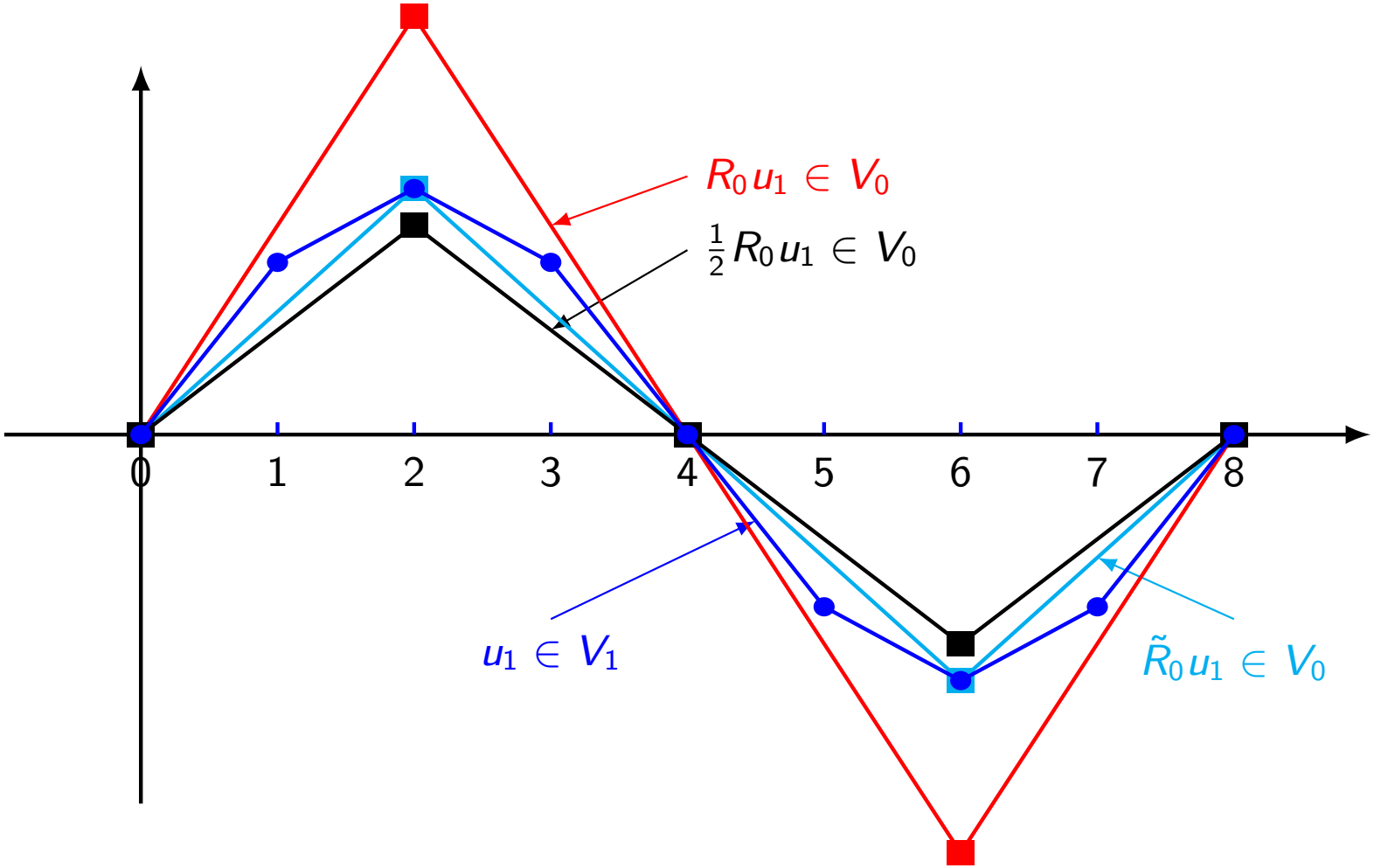

Figure: A Fine grid function, $u_1 \in V_1$, for $n_1 = 7$, and three possible restrictions $R_0 u_1 \in V_0$, $\frac{1}{2} R_0 u_1 \in V_0$, and $\tilde{R}_0 u_1 \in V_0$. The restriction $\frac{1}{2} R_0 u_1$ is called the full weighting restriction.

Other Restriction Matrices

To understand what is pictured in the figure on the last slide, we need to understand what is the action of R_0 on $\boldsymbol{u}_1$. If $\boldsymbol{u}_1 \in \mathbb{R}^{n_1}$ is the coordinate vector of $u_1 \in V_1$ with respect to the hat function basis B_1, then, clearly,

$$R_0 \boldsymbol{u}_1 = \begin{bmatrix} \frac{1}{2} & 1 & \frac{1}{2} & & & & \\ & & \frac{1}{2} & 1 & \frac{1}{2} & & \\ & & & & \frac{1}{2} & 1 & \frac{1}{2} \end{bmatrix} \begin{bmatrix} u_{1,1} \\ u_{1,2} \\ u_{1,3} \\ u_{1,4} \\ u_{1,5} \\ u_{1,6} \\ u_{1,7} \end{bmatrix} = \begin{bmatrix} \frac{1}{2}u_{1,1} + u_{1,2} + \frac{1}{2}u_{1,3} \\ \frac{1}{2}u_{1,3} + u_{1,4} + \frac{1}{2}u_{1,5} \\ \frac{1}{2}u_{1,5} + u_{1,6} + \frac{1}{2}u_{1,7} \end{bmatrix}.$$

The results of this calculation give coordinates that are twice the size that they should be in order to be geometrically and analytically sensible. Thus, dividing by 2, we get a more satisfying result.

Other Restriction Matrices

There is another possibility that might seem obvious. If $\boldsymbol{u}_1 \in \mathbb{R}^{n_1}$ is the coordinate vector of $u_1 \in V_1$ with respect to the hat function basis B_1, then, we could define

$$\tilde{\mathrm{R}}_0 \boldsymbol{u}_1 = \begin{bmatrix} 0 & 1 & 0 & & & & \\ & & 0 & 1 & 0 & & \\ & & & & 0 & 1 & 0 \end{bmatrix} \begin{bmatrix} u_{1,1} \\ u_{1,2} \\ u_{1,3} \\ u_{1,4} \\ u_{1,5} \\ u_{1,6} \\ u_{1,7} \end{bmatrix} = \begin{bmatrix} u_{1,2} \\ u_{1,4} \\ u_{1,6} \end{bmatrix}.$$

In the figure two slides ago, $\tilde{R}_0 u_1 \in V_0$ is the function whose coordinate representation in the basis B_0 is $\tilde{\mathrm{R}}_0 \boldsymbol{u}_1$. This too gives a more satisfying result than the standard restriction.

Definition (Full Weighting Restriction)

The matrix $\frac{1}{2}R_0$, where R_0 is defined as above, is called the **full weighting restriction matrix**.

Remark

Clearly, $\frac{1}{2}\mathrm{R}_0$ *and* $\tilde{\mathrm{R}}_0$ *seem to give more geometrically meaningful results than* R_0*. So, why do we not use them? The answer is simple, the Galerkin condition. If we use either* $\frac{1}{2}\mathrm{R}_0$ *or* $\tilde{\mathrm{R}}_0$*, the Galerkin condition will be broken, and it is too useful to dismiss, as we shall see.*

Fourier Error Analysis

Fourier Error Analysis

Recall the following result from the last chapter concerning the two-grid algorithm:

$$\boldsymbol{e}_1^{k+1} = \mathrm{E}_1 \boldsymbol{e}_1^k,$$

where

$$\mathrm{E}_1 = (\mathrm{K}_1^*)^{m_2} \left(\mathrm{I}_1 - \tilde{\Pi}_1 \right) (\mathrm{K}_1)^{m_1} .$$

Also, for the present case,

$$\mathrm{K}_1 = \mathrm{I}_1 - \omega_0 \frac{h_1}{2} \mathrm{A}_1 = \mathrm{K}_1^*.$$

$\tilde{\Pi}_1$ is the coarse grid Ritz projection matrix

$$\tilde{\Pi}_1 = \mathrm{R}_0^\top \mathrm{A}_0^{-1} \mathrm{R}_0 \mathrm{A}_1.$$

Assuming that the level-0 stiffness matrix A_0 satisfies the Galerkin condition, we have

$$\tilde{\Pi}_1^2 = \tilde{\Pi}_1.$$

Notation

We will use the following simplifying notation throughout this section:

$$\mathtt{C}_m := = \cos^2\left(\frac{m\pi h_1}{2}\right) = \frac{1}{2}(1+\cos(m\pi h_1)), \tag{1}$$

$$\mathtt{S}_m := = \sin^2\left(\frac{m\pi h_1}{2}\right) = \frac{1}{2}(1-\cos(m\pi h_1)). \tag{2}$$

Notation

Define

$$k' := n_1 + 1 - k. \tag{3}$$

See, for example, the table below for the relationship between k and k'.

k frequency characterization	k	$k' = n_1 + 1 - k$	k' frequency characterization
low	1	$7 = n_1$	high
low	2	6	high
low	3	5	high
high	$n_0 + 1 = 4$	$4 = n_0 + 1$	high
high	5	3	low
high	6	2	low
high	$n_1 = 7$	1	low

Table: The values of k' as a function of k for the case $n_1 = 7$, $n_0 = 3$.

Analysis of Fourier Modes

To analyze the error quantitatively, we need know what are the actions of our various matrices on the eigenvectors from the coarse and fine grids, which are denoted in the usual way,

$$\left[\boldsymbol{v}_\ell^{(k)}\right]_i = \sin(k\pi x_{\ell,i}), \quad 1 \le i, k \le n_\ell, \quad \ell = 0, 1,$$

where the grid points for the coarse and fine grids are determined via

$$x_{\ell,i} = i \cdot h_\ell, \quad \ell = 0, 1, \quad 0 \le i \le n_\ell + 1.$$

We begin by listing some aliasing-type results that will be needed in our Fourier analysis.

Lemma (Aliasing)

Suppose the two-level grid is uniform and nested. Then, for $1 \leq k \leq n_1$ *and* $1 \leq i \leq n_0$,

$$\sin(k'\pi x_{0,i}) = \left[\boldsymbol{v}_0^{(k')}\right]_i = -\left[\boldsymbol{v}_0^{(k)}\right]_i = -\sin(k\pi x_{0,i}. \tag{4}$$

Furthermore, for $1 \leq k \leq n_1$,

$$\cos\left(k'\pi h_1\right) = -\cos(k\pi h_1). \tag{5}$$

Finally, for $1 \leq k \leq n_1$ *and* $1 \leq i \leq n_1$,

$$\sin(k'\pi x_{1,i}) = \left[\boldsymbol{v}_1^{(k')}\right]_i = (-1)^{i+1}\left[\boldsymbol{v}_1^{(k)}\right]_i = (-1)^{i+1}\sin(k\pi x_{1,i}). \tag{6}$$

Proof.

First, observe that, for any $1 \leq k \leq n_1$,

$$\begin{aligned}
\left[\boldsymbol{v}_0^{(k')}\right]_i &= \left[\boldsymbol{v}_0^{(n_1+1-k)}\right]_i \\
&= \sin\left((n_1+1-k)\pi i h_0\right) \\
&= \sin\left((n_1+1-k)\pi \frac{2i}{n_1+1}\right) \\
&= \sin\left(2\pi i - k\pi x_{0,i}\right) \\
&= \sin\left(-k\pi x_{0,i}\right) \\
&= -\sin\left(k\pi x_{0,i}\right) \\
&= -\left[\boldsymbol{v}_0^{(k)}\right]_i,
\end{aligned}$$

which quantifies the phenomenon known as *aliasing*, that is, high frequency modes (sine waves) are distorted on a coarse grid.

Proof (Cont.)

Similarly,

$$\begin{aligned}\cos\left(k'\pi h_1\right) &= \cos\left((n_1+1-k)\pi h_1\right)\\ &= \cos\left(\pi - k\pi h_1\right)\\ &= -\cos(k\pi h_1).\end{aligned}$$

To see the last result, consider

$$\begin{aligned}\left[\boldsymbol{v}_1^{(k')}\right]_i &= \sin\left((n_1+1-k)\pi x_{1,i}\right)\\ &= \sin\left((n_1+1-k)\pi\frac{i}{n_1+1}\right)\\ &= \sin\left(i\pi - k\pi x_{1,i}\right).\end{aligned}$$

□

Proposition (Restriction Modal Analysis)

Suppose that the two-level grid is uniform and nested. Then

$$\mathrm{R}_0 \boldsymbol{v}_1^{(k)} = \begin{cases} 2\mathrm{C}_k \boldsymbol{v}_0^{(k)}, & 1 \le k \le n_0, \\ -2\mathrm{S}_{k'} \boldsymbol{v}_0^{(k')}, & n_0 + 1 \le k \le n_1. \end{cases} \tag{7}$$

Proof.

(Low frequency components): Consider for $1 \le i \le n_0$, $1 \le k \le n_0$,

$$
\begin{aligned}
\left[R_0 \boldsymbol{v}_1^{(k)}\right]_i &= \frac{1}{2}\left\{\sin(k\pi x_{1,2i-1}) + 2\sin(k\pi x_{1,2i}) + \sin(k\pi x_{1,2i+1})\right\} \\
&= \frac{1}{2}\Big[\sin(k\pi x_{1,2i} - k\pi h_1) + 2\sin(k\pi x_{1,2i}) \\
&\quad + \sin(k\pi x_{1,2i} + k\pi h_1)\Big] \\
&= \frac{1}{2}\Big[\sin(k\pi x_{1,2i})\cos(k\pi h_1) - \cos(k\pi x_{1,2i})\sin(k\pi h_1) \\
&\quad + \sin(k\pi x_{1,2i})\cos(k\pi h_1) + \cos(k\pi x_{1,2i})\sin(k\pi h_1) \\
&\quad + 2\sin(k\pi x_{1,2i})\Big] \\
&= \sin(k\pi x_{1,2i})\cos(k\pi h_1) + \sin(k\pi x_{1,2i}) \\
&= \sin(k\pi x_{1,2i})(\cos(k\pi h_1) + 1) \\
&= 2\cos^2\left(\frac{k\pi h_1}{2}\right)\sin(k\pi x_{1,2i}) \\
&= 2c_k\left[\boldsymbol{v}_0^{(k)}\right]_i .
\end{aligned}
$$

The first part is complete.

Proof (Cont.)

(High frequency components): The first part of the calculation above is still valid for $n_0 + 1 \leq k \leq n_1$. We now use the aliasing results (4) and (5) from the technical lemma to obtain

$$\begin{aligned}
\left[R_0 \boldsymbol{v}_1^{(k)}\right]_i &= \frac{1}{2}\left\{\sin(k\pi x_{1,2i-1}) + 2\sin(k\pi x_{1,2i}) + \sin(k\pi x_{1,2i+1})\right\} \\
&= \sin(k\pi x_{1,2i})(\cos(k\pi h_1) + 1) \\
&= (\cos(k\pi h_1) + 1)\left[\boldsymbol{v}_0^{(k)}\right]_i \\
&= -(1 - \cos(k'\pi h_1))\left[\boldsymbol{v}_0^{(k')}\right]_i \\
&= -2\sin^2\left(\frac{k'\pi h_1}{2}\right)\left[\boldsymbol{v}_0^{(k')}\right]_i \\
&= -2S_{k'}\left[\boldsymbol{v}_0^{(k')}\right]_i,
\end{aligned}$$

where we have used the aliasing calculations above. The result is proved. □

Proposition (Prolongation Modal Analysis)

Suppose that the two-level grid is uniform and nested. For $1 \leq k \leq n_0$,

$$\mathrm{P}_0 \boldsymbol{v}_0^{(k)} = \mathtt{C}_k \boldsymbol{v}_1^{(k)} - \mathtt{S}_k \boldsymbol{v}_1^{(k')}. \tag{8}$$

Proof.

Now, for $1 \leq i \leq n_1$, define

$$j := \begin{cases} \frac{i+1}{2}, & \text{if } i \text{ is odd,} \\ \frac{i}{2}, & \text{if } i \text{ is even.} \end{cases}$$

Proof (Cont.)

Working with the right hand side of the desired result, for $1 \leq i \leq n_1$, and $1 \leq k \leq n_0$, it follows that

$$
\begin{aligned}
I_i^{(k)} &:= \mathtt{C}_k \left[\boldsymbol{v}_1^{(k)}\right]_i - \mathtt{S}_k \left[\boldsymbol{v}_1^{(k')}\right]_i \\
&= \begin{cases} \cos(k\pi h_1)\sin(k\pi x_{1,i}), & i \text{ is odd}, \\ \sin(k\pi x_{1,i}), & i \text{ is even}, \end{cases} \qquad \text{((6) and basic trigonometry)} \\
&= \begin{cases} \cos(k\pi h_1)\sin(k\pi x_{1,2j-1}), & i \text{ is odd}, \\ \sin(k\pi x_{1,2j}), & i \text{ is even}, \end{cases} \\
&= \begin{cases} \frac{1}{2}\sin(k\pi x_{1,2j-1} + k\pi h_1) + \frac{1}{2}\sin(k\pi x_{1,2j-1} - k\pi h_1), & i \text{ is odd}, \\ \sin(k\pi x_{1,2j}), & i \text{ is even}, \end{cases} \\
&= \begin{cases} \frac{1}{2}\sin(k\pi x_{1,2j}) + \frac{1}{2}\sin(k\pi x_{1,2j-2}), & i \text{ is odd}, \\ \sin(k\pi x_{1,2j}), & i \text{ is even}, \end{cases} \\
&= \begin{cases} \left[\mathtt{P}_0 \boldsymbol{v}_0^{(k)}\right]_{2j-1}, & i \text{ is odd}, \\ \left[\mathtt{P}_0 \boldsymbol{v}_0^{(k)}\right]_{2j}, & i \text{ is even}. \end{cases}
\end{aligned}
$$

Proof (Cont.)

Thus

$$I_i^{(k)} = \mathrm{C}_k \left[\boldsymbol{v}_1^{(k)} \right]_i - \mathrm{S}_k \left[\boldsymbol{v}_1^{(k')} \right]_i = \left[\mathrm{P}_0 \boldsymbol{v}_0^{(k)} \right]_i .$$

Proposition (Galerkin Projection Modal Analysis)

Suppose that the two-level grid is uniform and nested and A_0 *satisfies the Galerkin condition. Then*

$$(I_1 - \tilde{\Pi}_1)\boldsymbol{v}_1^{(k)} = S_k \boldsymbol{v}_1^{(k)} + S_k \boldsymbol{v}_1^{(k')}, \tag{9}$$

for $1 \leq k \leq n_0$. *Similarly,*

$$(I_1 - \tilde{\Pi}_1)\boldsymbol{v}_1^{(k')} = C_k \boldsymbol{v}_1^{(k)} + C_k \boldsymbol{v}_1^{(k')}, \tag{10}$$

for $1 \leq k \leq n_0 + 1$.

Proof.

Recall that

$$\tilde{\Pi}_1 = P_0 A_0^{-1} R_0 A_1 \in \mathbb{R}^{n_1 \times n_1},$$

where, since A_0 satisfies the Galerkin condition,

$$A_0 = R_0 A_1 P_0 \in \mathbb{R}^{n_0 \times n_0}.$$

Then, for $1 \leq k \leq n_0$,

$$\begin{aligned}
\tilde{\Pi}_1 \boldsymbol{v}_1^{(k)} &= P_0 A_0^{-1} R_0 A_1 \boldsymbol{v}_1^{(k)} \\
&= \lambda_1^{(k)} P_0 A_0^{-1} R_0 \boldsymbol{v}_1^{(k)} \\
&\overset{(7)}{=} 2 C_k \lambda_1^{(k)} P_0 A_0^{-1} \boldsymbol{v}_0^{(k)} \\
&= \frac{2 C_k \lambda_1^{(k)}}{\lambda_0^{(k)}} P_0 \boldsymbol{v}_0^{(k)} \\
&\overset{(8)}{=} \frac{2 C_k \lambda_1^{(k)}}{\lambda_0^{(k)}} \left\{ C_k \boldsymbol{v}_1^{(k)} - S_k \boldsymbol{v}_1^{(k')} \right\}.
\end{aligned}$$

Proof (Cont.)

Observe,

$$\begin{aligned}\frac{\lambda_1^{(k)}}{\lambda_0^{(k)}} &= \frac{\frac{2}{h_1}\left(1-\cos(k\pi h_1)\right)}{\frac{2}{h_0}\left(1-\cos(k\pi h_0)\right)} \\ &= \frac{h_0}{h_1}\frac{\sin^2\left(\frac{k\pi h_1}{2}\right)}{\sin^2(k\pi h_1)} \\ &= \frac{2\mathtt{S}_k}{\sin^2(k\pi h_1)}.\end{aligned}$$

Thus

$$\tilde{\Pi}_1 \boldsymbol{v}_1^{(k)} = \frac{4\mathtt{C}_k\mathtt{S}_k}{\sin^2(k\pi h_1)}\left\{\mathtt{C}_k \boldsymbol{v}_1^{(k)} - \mathtt{S}_k \boldsymbol{v}_1^{(k')}\right\}.$$

But

$$\mathtt{C}_k\mathtt{S}_k = \frac{1}{4}\sin^2(k\pi h_1),$$

as the reader can easily check. We have

$$\tilde{\Pi}_1 \boldsymbol{v}_1^{(k)} = \mathtt{C}_k \boldsymbol{v}_1^{(k)} - \mathtt{S}_k \boldsymbol{v}_1^{(k')}, \quad 1 \le k \le n_0.$$

Proof (Cont.)

Therefore, for $1 \leq k \leq n_0$,

$$\begin{aligned}(\mathrm{I}_1 - \tilde{\Pi}_1)\boldsymbol{v}_1^{(k)} &= (1 - \mathrm{C}_k)\boldsymbol{v}_1^{(k)} + \mathrm{S}_k \boldsymbol{v}_1^{(k')} \\ &= \mathrm{S}_k \left(\boldsymbol{v}_1^{(k)} + \boldsymbol{v}_1^{(k')}\right),\end{aligned}$$

which is (9). Equation (10) is established in an analogous way. □

For our convergence result, we will consider the one-sided two-grid algorithm, that is, the usual two-grid algorithm with no post-smoothing, $m_2 = 0$. This non-symmetric version of the algorithm works perfectly well, as we shall see, for the quantitative Fourier analysis that we are using. Other forms of analysis will require the symmetry.

Theorem (Convergence of the One-Sided Two-Grid Algorithm)

Suppose that the two-level grid is uniform and nested and A_0 *satisfies the Galerkin condition. Assume that* $m_2 = 0$, $\omega_0 = \frac{2}{3}$, *and* $m_1 \geq 1$. *Then*

$$\left\| \boldsymbol{e}_1^{\ell+1} \right\|_1 \leq \left\{ \frac{1}{2} + \frac{1}{3^{m_1}} \right\}^{1/2} \left\| \boldsymbol{e}_1^{\ell} \right\|_1 .$$

Proof.

We begin with the basis expansion

$$\boldsymbol{e}_1^{\ell} = \sum_{k=1}^{n_1} \epsilon_k \boldsymbol{v}_1^{(k)}.$$

The error transfer matrix, E_1, for the two-grid scheme, in this case, satisfies

$$\boldsymbol{e}_1^{\ell+1} = \mathsf{E}_1 \boldsymbol{e}_1^{\ell},$$

where

$$\mathsf{E}_1 = (\mathsf{I}_1 - \tilde{\Pi}_1)\mathsf{K}_1^{m_1}.$$

Hence,

$$\boldsymbol{e}_1^{\ell+1} = \sum_{k=1}^{n_1} \epsilon_k (\mathsf{I}_1 - \tilde{\Pi}_1)\mathsf{K}_1^{m_1} \boldsymbol{v}_1^{(k)}.$$

Proof (Cont.)

By the Galerkin Projection Modal Analysis, for $1 \leq k \leq n_0 + 1$,

$$(\mathrm{I}_1 - \tilde{\Pi}_1)\mathrm{K}_1^{m_1} \boldsymbol{v}_1^{(k)} = \alpha_k \left\{ \boldsymbol{v}_1^{(k)} + \boldsymbol{v}_1^{(k')} \right\}, \tag{11}$$

and, for $1 \leq k \leq n_0 + 1$,

$$(\mathrm{I}_1 - \tilde{\Pi}_1)\mathrm{K}_1^{m_1} \boldsymbol{v}_1^{(k')} = \beta_k \left\{ \boldsymbol{v}_1^{(k)} + \boldsymbol{v}_1^{(k')} \right\}, \tag{12}$$

where

$$\alpha_k := \left(\mu_1^{(k)}(\omega_0) \right)^{m_1} \mathtt{S}_k, \quad 1 \leq k \leq n_0 + 1,$$

and

$$\beta_k := \left(\mu_1^{(k')}(\omega_0) \right)^{m_1} \mathtt{C}_k, \quad 1 \leq k \leq n_0 + 1.$$

Proof (Cont.)

Observe that we have extended the upper limit of the index k in (11) by 1, up to $k = n_0 + 1$. The result is still valid in this case. Further, observe that

$$\alpha_{n_0+1} = \beta_{n_0+1},$$

as the reader can easily verify.
With the optimal choice of ω_0 of the damped Jacobi method derived in the last chapter, we have

$$\left|\mu_1^{(k)}(\omega_0)\right| \leq \frac{1}{3}, \quad n_0 + 1 \leq k \leq n_1 \quad \text{(high frequencies)},$$

and

$$\left|\mu_1^{(k)}(\omega_0)\right| < 1, \quad 1 \leq k \leq n_1 \quad \text{(all frequencies)}.$$

Proof (Cont.)

We can estimate α_k and β_k as follows:

$$|\alpha_k| \leq 1^{m_1} \mathtt{S}_k \leq 1 \cdot \frac{1}{2}, \quad 1 \leq k \leq n_0 + 1,$$

and

$$|\beta_k| \leq \left(\frac{1}{3}\right)^{m_1} \mathtt{C}_k \leq \left(\frac{1}{3}\right)^{m_1} \cdot 1, \quad 1 \leq k \leq n_0 + 1.$$

We can represent the error as

$$\begin{aligned} \boldsymbol{e}_1^{\ell+1} &= \mathtt{E}_1 \boldsymbol{e}_1^{\ell} \\ &= \sum_{k=1}^{n_0+1} \delta_k \left(\epsilon_k \alpha_k + \epsilon_{k'} \beta_k\right) \left(\boldsymbol{v}_1^{(k)} + \boldsymbol{v}_1^{(k')}\right), \end{aligned}$$

where

$$\delta_k = \begin{cases} \frac{1}{2}, & k = n_0 + 1, \\ 1, & \text{otherwise}, \end{cases}$$

which reconciles the double counting of the term indexed $k = n_0 + 1$.

Proof (Cont.)

Now, notice that the eigenvectors satisfy the orthogonality condition

$$\begin{aligned}\left(\boldsymbol{v}_1^{(i)}, \boldsymbol{v}_1^{(j)}\right)_1 &= \sum_{m=1}^{n_1} \sin(i\pi x_{1,m}) \sin(j\pi x_{1,m}) \\ &= \delta_{ij} \frac{n_1 + 1}{2}.\end{aligned}$$

Proof (Cont.)

Therefore,

$$
\begin{aligned}
\left\| \boldsymbol{e}_1^{\ell+1} \right\|_1^2 &= \left(\boldsymbol{e}_1^{\ell+1}, \boldsymbol{e}_1^{\ell+1} \right)_1 \\
&= (n_1+1) \sum_{k=1}^{n_0+1} \delta_k \left(\epsilon_k^2 \alpha_k^2 + \epsilon_{k'}^2 \beta_k^2 + 2\epsilon_k \epsilon_{k'} \alpha_k \beta_k \right) \\
&\overset{\text{AGMI}}{\leq} (n_1+1) \sum_{k=1}^{n_0+1} \delta_k \left\{ \epsilon_k^2 \alpha_k^2 + \epsilon_{k'}^2 \beta_k^2 + \left(\epsilon_k^2 + \epsilon_{k'}^2 \right) |\alpha_k| \, |\beta_k| \right\} \\
&\leq (n_1+1) \sum_{k=1}^{n_0+1} \delta_k \left\{ \epsilon_k^2 \left(\frac{1}{2} \right)^2 + \epsilon_{k'}^2 \left(\frac{1}{3} \right)^{2m_1} \right. \\
&\qquad \left. + (\epsilon_k^2 + \epsilon_{k'}^2) \frac{1}{2} \left(\frac{1}{3} \right)^{m_1} \right\} \\
&= (n_1+1) \sum_{k=1}^{n_0+1} \delta_k \left\{ \epsilon_k^2 \left(\left(\frac{1}{2} \right)^2 + \frac{1}{2} \left(\frac{1}{3} \right)^{m_1} \right) \right. \\
&\qquad \left. + \epsilon_{k'}^2 \left(\left(\frac{1}{3} \right)^{2m_1} + \frac{1}{2} \left(\frac{1}{3} \right)^{m_1} \right) \right\}.
\end{aligned}
$$

Proof (Cont.)

Since,

$$\left(\frac{1}{3}\right)^{m_1} \leq \frac{1}{2},$$

we have

$$\begin{aligned}\left\|\boldsymbol{e}_1^{\ell+1}\right\|_1^2 &\leq \frac{n_1+1}{2}\left\{\frac{1}{2}+\left(\frac{1}{3}\right)^{m_1}\right\}\sum_{k=1}^{n_0+1}\delta_k\left(\epsilon_k^2+\epsilon_{k'}^2\right)\\ &= \left\{\frac{1}{2}+\left(\frac{1}{3}\right)^{m_1}\right\}\left\|\boldsymbol{e}_1^{\ell}\right\|_1^2.\end{aligned}$$

Finally,

$$\left\|\boldsymbol{e}_1^{\ell+1}\right\|_1 \leq \gamma(m_1)\left\|\boldsymbol{e}_1^{\ell}\right\|_1,$$

where

$$\gamma(m_1) := \left\{\frac{1}{2}+\left(\frac{1}{3}\right)^{m_1}\right\}^{1/2}. \tag{13}$$

□

m_1	1	2	3	$\cdots$	∞
$\gamma(m_1)$	0.91287	0.78176	0.73283	$\cdots$	0.70710

Table: Numerical values of $\gamma(m_1)$, defined in Equation (13), for certain values of the pre-smoothing number, m_1. It does not make much sense to use $m_1 > 3$, since the geometric convergence rate does not significantly improve, at least theoretically.

Remark

The key observation is that $\gamma(m_1)$ is h_1 independent. See the table above for guidance on choosing m_1.

Some Computational Experiments

To conclude this chapter, let us perform some computational experiments to confirm the predicted convergence results. In particular, let us use the one-sided two-grid algorithm to approximate the solution of

$$\mathrm{A}_1 \boldsymbol{u}_1^{\mathrm{E}} = \boldsymbol{f}_1,$$

where A_1 is the standard finite element stiffness matrix, defined in

$$a_{1,i,j} = \left(\psi'_{1,j}, \psi'_{1,i}\right)_{L^2(0,1)} = \left(\psi'_{1,i}, \psi'_{1,j}\right)_{L^2(0,1)} \tag{14}$$

for the model problem

$$\begin{cases} -u'' &= f, \quad \text{in} \quad \Omega = (0,1), \\ u &= 0, \quad \text{on} \quad \partial\Omega = \{0,1\}. \end{cases} \tag{15}$$

In our experiments, we specify the exact solution:

$$\left[\boldsymbol{u}_1^{\mathrm{E}}\right]_i = u_{1,i}^{\mathrm{E}} = \exp(\sin(3.0\pi * x_{1,i})) - 1.0.$$

In other words, we manufacture the force vector by setting $\boldsymbol{f}_1 := \mathrm{A}_1 \boldsymbol{u}_1^{\mathrm{E}}$. We report on four particular computational experiments in the figures on the next two slides and a number of other experiments in the coming table. The initial approximation, $\boldsymbol{u}_1^{(0)}$, is chosen via pseudorandom number selection. The Matlab code is listed in the book file.

Experiment 1

In experiment 1, we use the parameters $\omega = 2/3$ and $m_1 = 3$. The results are posted in the figures on the next three slides. The error reduction is plotted as a function of iteration, k, in the next figure. The computed error reduction factor, γ_{comp}, is much better than the theoretically predicted value, almost 10 times smaller. This contraction factor is computed using a log-linear fit of the last four error values,

$$\left\| \boldsymbol{u}_1^{\mathrm{E}} - \boldsymbol{u}_1^{\ell} \right\|_1, \quad \ell = k_\star - 3, k_\star - 2, k_\star - 1, k_\star,$$

where $k_\star$ is that value of k at which the stopping tolerance is reached. For our experiments, the stopping tolerance is achieved when

$$\left\| \boldsymbol{u}_1^{\mathrm{E}} - \boldsymbol{u}_1^{k_\star} \right\|_1 \leq 1.0 \times 10^{-09}.$$

Stopping using the exact error is not practical. But our, computations show that the norm of the coarse grid correction is a good indicator of the error.

Experiment 1

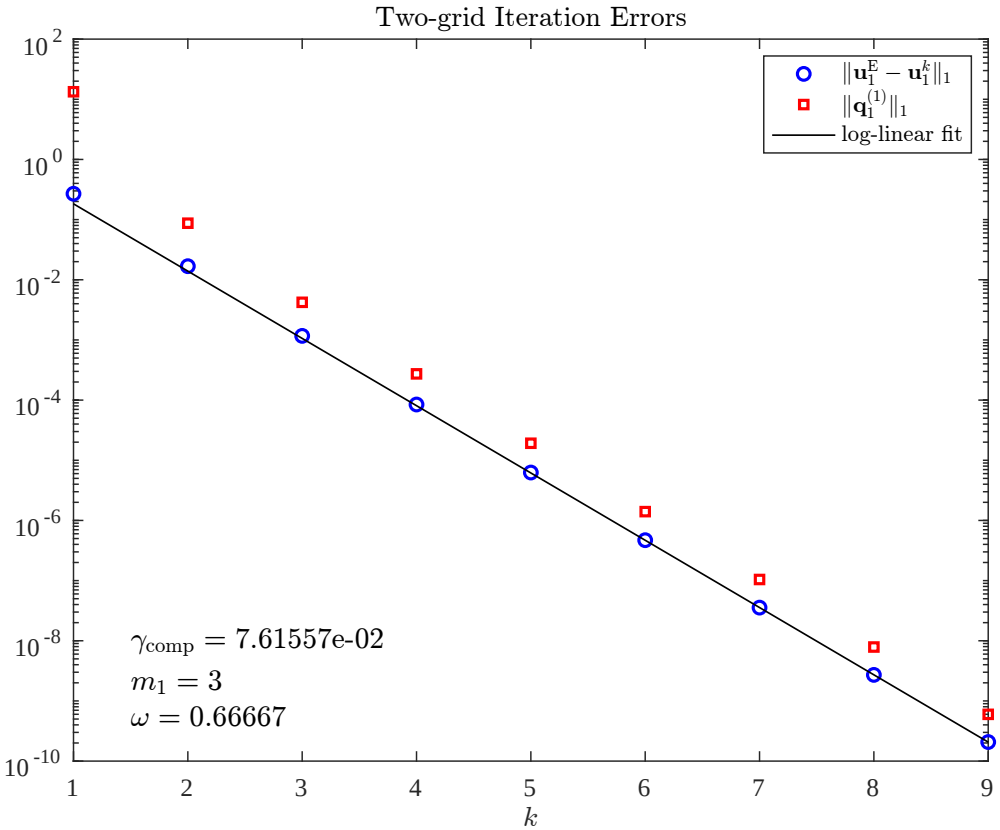

Figure: The error reduction for the one-sided two-grid algorithm, using the parameters $\omega = 2/3$, $m_1 = 3$, and $n_1 = 255$. The computed error reduction factor, γ_{comp}, is much better than the theoretically predicted value, almost 10 times smaller. The factor γ_{comp} is computed using a log-linear fit of the last four error values. Note that the norm of the coarse grid correction is a good indicator of the error.

Experiment 1

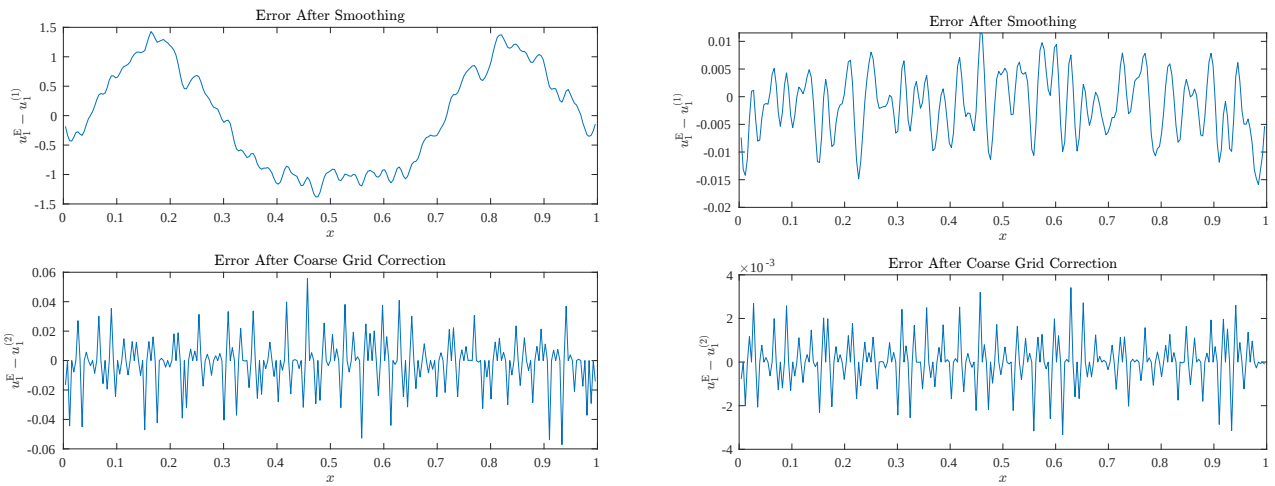

Figure: The errors after pre-smoothing and after coarse grid correction for the one-sided two-grid algorithm at iterations $k = 1$ (left two plots) and $k = 2$ (right two plots), using the parameters $\omega = 2/3$, $m_1 = 3$, and $n_1 = 255$. See the figure one slide ago.

The error function after pre-smoothing, $u_1^{\mathrm{E}}(x_{1,i}) - u_1^{(1)}(x_{1,i})$, and after coarse grid correction, $u_1^{\mathrm{E}}(x_{1,i}) - u_1^{(2)}(x_{1,i})$, for iterations $k = 1$ through $k = 4$. Notice that the smoothing operation really does "smooth" the error. Applying the coarse grid correction then drastically reduces the error, but it reintroduces some high frequency error. These are later squashed by smoothing, et cetera.

Experiment 1

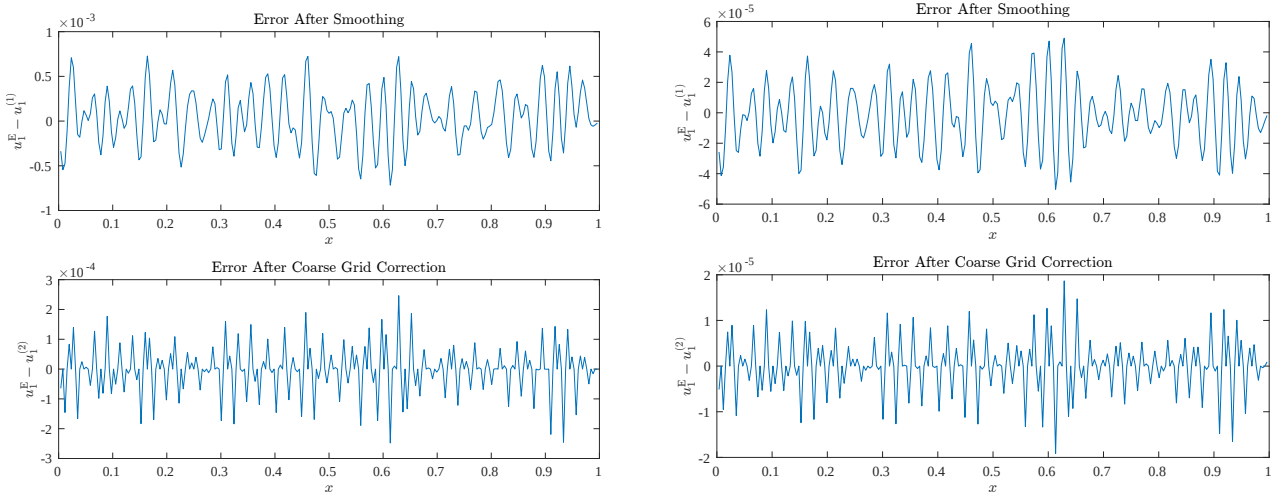

Figure: The errors after pre-smoothing and after coarse grid correction for the one-sided two-grid algorithm at iterations $k = 3$ (left two plots) and $k = 4$ (right two plots), using the parameters $\omega = 2/3$, $m_1 = 3$, and $n_1 = 255$. See the figure two slides ago.

The error function after pre-smoothing, $u_1^{\mathrm{E}}(x_{1,i}) - u_1^{(1)}(x_{1,i})$, and after coarse grid correction, $u_1^{\mathrm{E}}(x_{1,i}) - u_1^{(2)}(x_{1,i})$, for iterations $k = 1$ through $k = 4$. Notice that the smoothing operation really does "smooth" the error. Applying the coarse grid correction then drastically reduces the error, but it reintroduces some high frequency error. These are later squashed by smoothing, et cetera.

Experiment 2

In experiment 2, we use the parameters $\omega = 2/3$ and $m_1 = 10$. The error reduction is plotted as a function of the two-grid iteration number, k, in the figure on the next page. The computed error contraction factor γ_{comp} is calculated as in experiment 1, and is smaller than the factor from experiment 1. Doing more smoothing iterations reduces the error contraction factor γ_{comp}, but there is a diminishing return with this effort.

Experiment 2

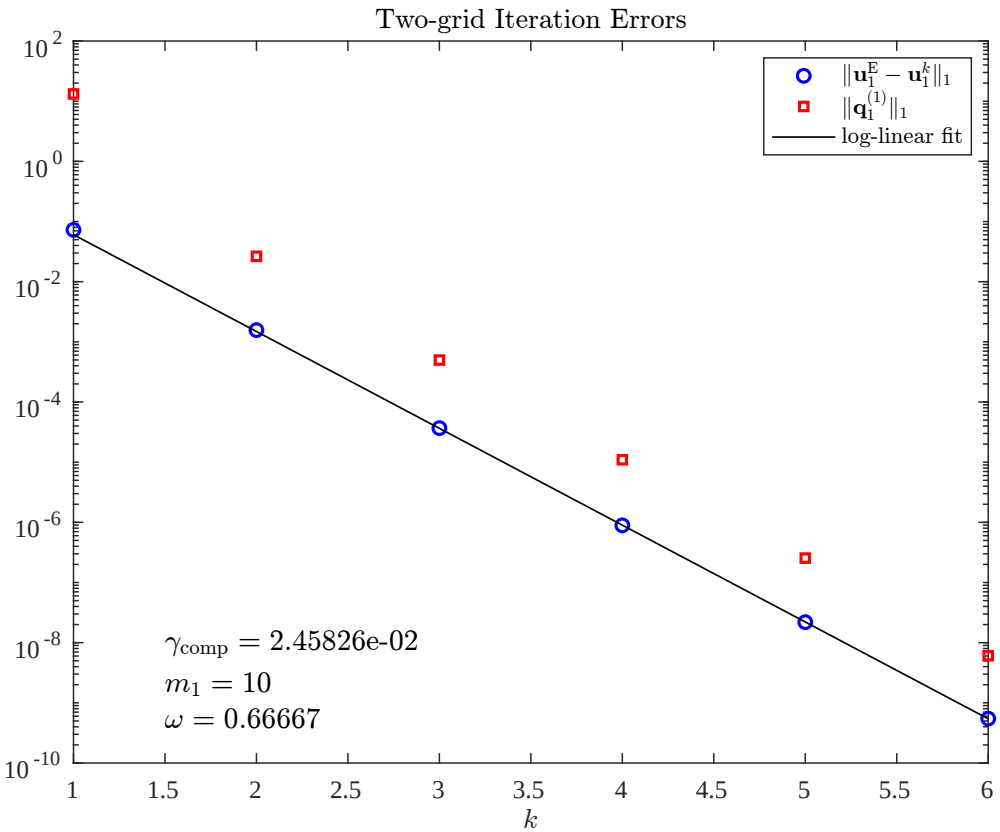

Figure: The error reduction for the one-sided two-grid algorithm, using the parameters $\omega = 2/3$, $m_1 = 10$, and $n_1 = 255$. The factor γ_{comp} is computed using a log-linear fit of the last four error values. Compare this rate with that from Figure 2.

Experiment 3

In experiment 3, we use the parameters $\omega = 1/2$ and $m_1 = 3$. The computed error contraction factor γ_{comp} is larger than that of experiment 1. In the next chapter, we will discuss the use of the parameter $\omega = 1/2$ in the damped Jacobi smoother. See the table at the end of the slides for the computed error contraction factors, γ_{comp}, for several different values of ω.

Experiment 3

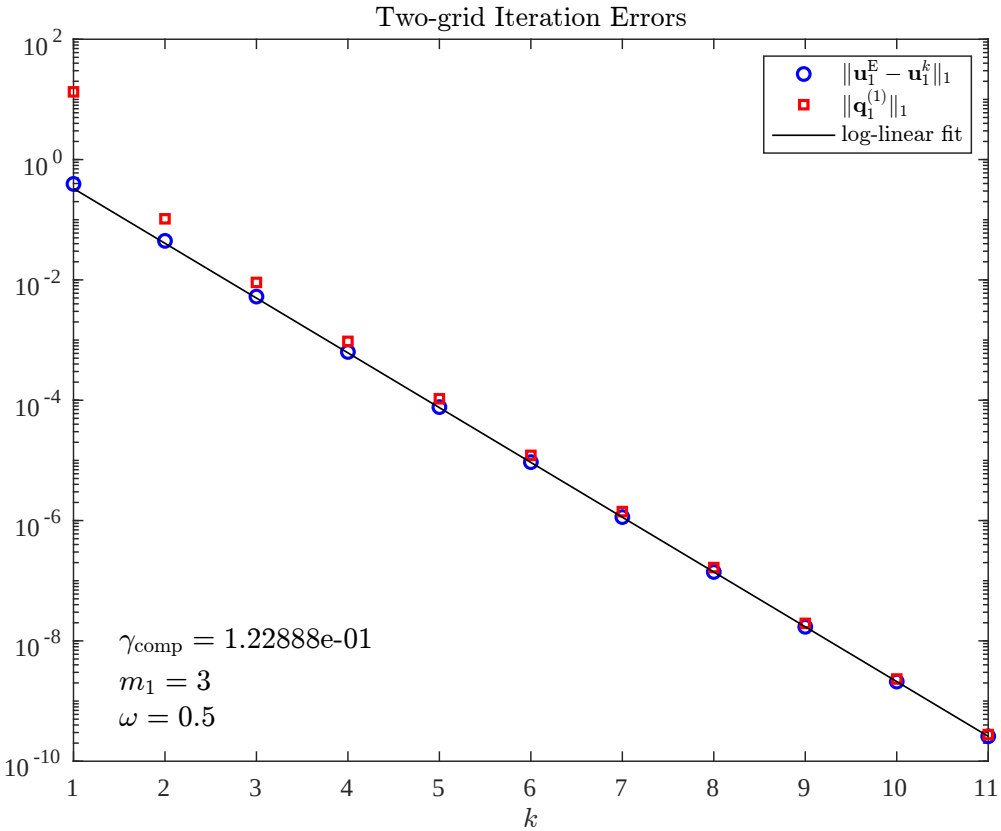

Figure: The error reduction for the one-sided two-grid algorithm, using the parameters $\omega = 1/2$, $m_1 = 3$, and $n_1 = 255$. The factor γ_{comp} is computed using a log-linear fit of the last four error values. Compare to experiment 1, and it appears that $\omega = 0.5$ is not optimal.

Experiment 4

In experiment 4, we use the parameters $\omega = 2/3$ and $m_1 = 20$. The error reduction is plotted as a function of the two-grid iteration number, k, in the figure on the next page. The computed error contraction factor γ_{comp} is calculated as in experiment 1, and is smaller than that computed in experiments 1 ($m_1 = 3$) and 2 ($m_1 = 10$).

Experiment 4

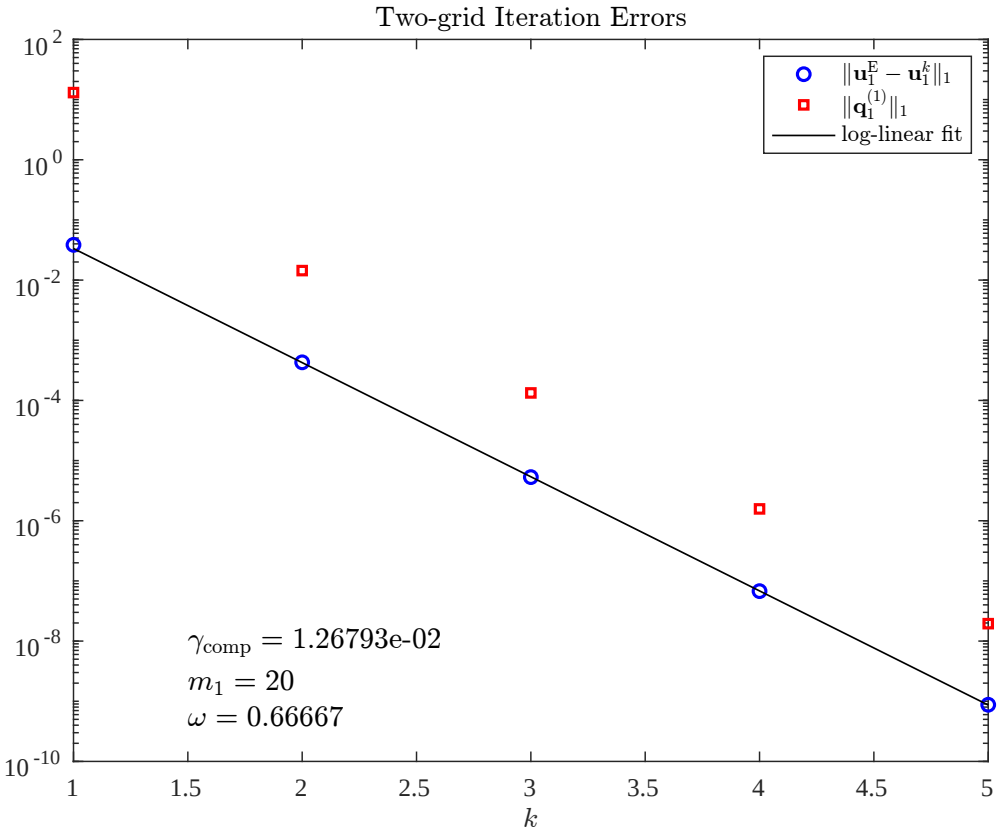

Figure: The error reduction for the one-sided two-grid algorithm, using the parameters $\omega = 2/3$, $m_1 = 20$, and $n_1 = 255$. The factor γ_{comp} is computed using a log-linear fit of the last four error values. Compare this rate with those from Figures 2 and 6. There is a diminishing return for doing more pre-smoothing steps. The convergence factor γ_{comp} is reduced, but not by much. See the table on the last page.

Experiment 4

Doing 20 pre-smoothing steps is not practical. But this experiment shows the (exaggerated) smoothing effect of the damped Jacobi method with a large number of pre-smoothing steps. See the figures on the next two pages.

Experiment 4

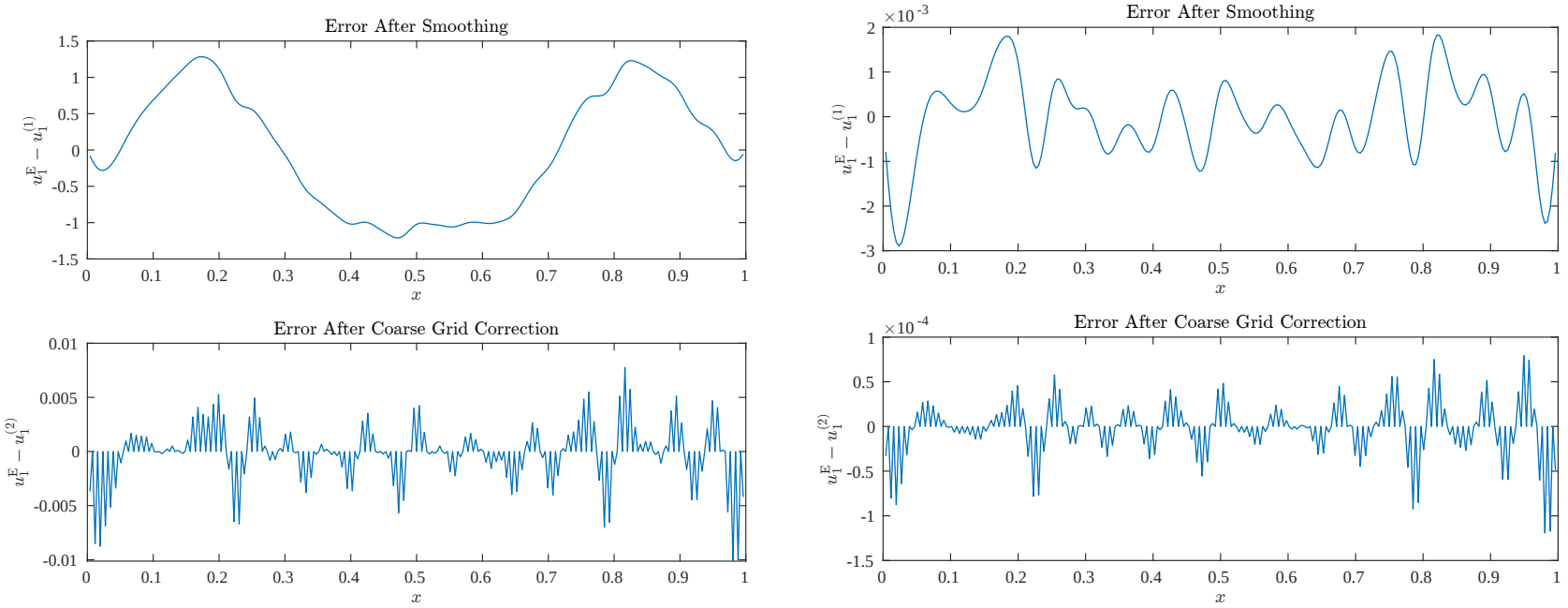

Figure: The errors after pre-smoothing and after coarse grid correction for the one-sided two-grid algorithm at iterations $k = 1$ (left two plots) and $k = 2$ (right two plots), using the parameters $\omega = 2/3$, $m_1 = 20$, and $n_1 = 255$. This is an exaggerated number of pre-smoothing steps. Compare with experiment 1.

Experiment 4

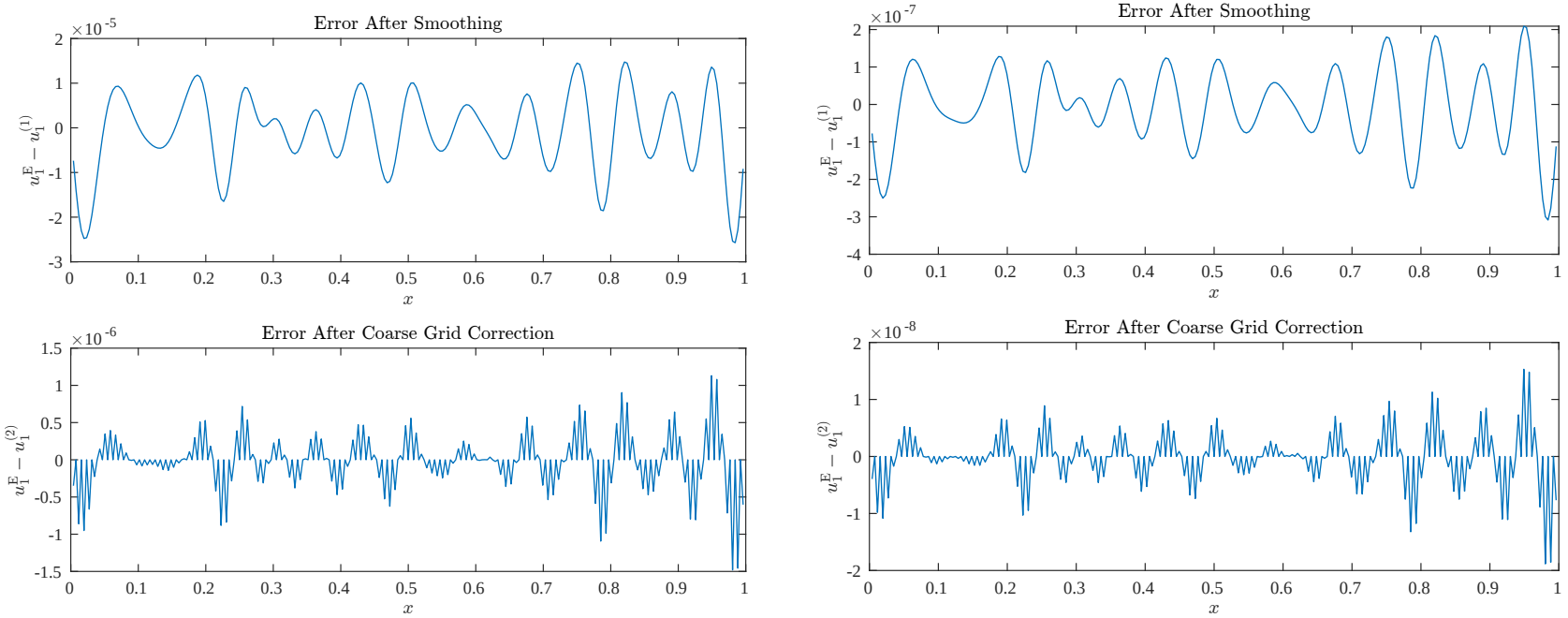

Figure: The errors after pre-smoothing and after coarse grid correction for the one-sided two-grid algorithm at iterations $k = 3$ (left two plots) and $k = 4$ (right two plots), using the parameters $\omega = 2/3$, $m_1 = 20$, and $n_1 = 255$. This is an exaggerated number of pre-smoothing steps. Compare with Figure 4. We use this this exaggeration to show the error "smoothing" effect of the pre-smoothing operation.

Summary of the experiments

Finally, a number of further computational experiments are summarized in the table at the end of the slides. We report only the computed contraction factor γ_{comp}. Doing experiments like this for known solutions can help users tune the parameters in their codes for close-to-optimal performance.

Summary of the experiments

n_1	ω	m_1	γ_{comp}
63	2/3	3	7.48×10^{-02}
127	2/3	3	7.50×10^{-02}
255	2/3	3	7.62×10^{-02}
511	2/3	3	7.55×10^{-02}
1023	2/3	3	7.50×10^{-02}
127	2/3	5	4.84×10^{-02}
127	2/3	7	3.54×10^{-02}
127	2/3	9	2.70×10^{-02}
127	2/3	11	2.22×10^{-02}
127	2/3	13	1.88×10^{-02}
127	2/3	15	1.62×10^{-02}
127	0.40	3	2.12×10^{-01}
127	0.45	3	1.62×10^{-01}
127	0.50	3	1.23×10^{-01}
127	0.55	3	9.75×10^{-02}
127	0.60	3	8.47×10^{-02}
127	0.65	3	7.73×10^{-02}
127	0.70	3	6.91×10^{-02}
127	0.75	3	1.22×10^{-01}
127	0.80	3	2.13×10^{-01}

Table: Computed two-grid convergence factors, γ_{comp}, for various parameter choices. The factor γ_{comp} is computed using a log-linear fit of the last four error values $\left\| \boldsymbol{u}_1^{\text{E}} - \boldsymbol{u}_1^k \right\|_1$.